FERMILAB-PUB-10-393-E

Search for pair production of the scalar top quark in the electron+muon final state

V.M. Abazov,[35] B. Abbott,[73] M. Abolins,[62] B.S. Acharya,[29] M. Adams,[48] T. Adams,[46] G.D. Alexeev,[35] G. Alkhazov,[39] A. Alton[a],[61] G. Alverson,[60] G.A. Alves,[2] L.S. Ancu,[34] M. Aoki,[47] Y. Arnoud,[14] M. Arov,[57] A. Askew,[46] B. Åsman,[40] O. Atramentov,[65] C. Avila,[8] J. BackusMayes,[80] F. Badaud,[13] L. Bagby,[47] B. Baldin,[47] D.V. Bandurin,[46] S. Banerjee,[29] E. Barberis,[60] P. Baringer,[55] J. Barreto,[2] J.F. Bartlett,[47] U. Bassler,[18] V. Bazterra,[48] S. Beale,[6] A. Bean,[55] M. Begalli,[3] M. Begel,[71] C. Belanger-Champagne,[40] L. Bellantoni,[47] S.B. Beri,[27] G. Bernardi,[17] R. Bernhard,[22] I. Bertram,[41] M. Besançon,[18] R. Beuselinck,[42] V.A. Bezzubov,[38] P.C. Bhat,[47] V. Bhatnagar,[27] G. Blazey,[49] S. Blessing,[46] K. Bloom,[64] A. Boehnlein,[47] D. Boline,[70] T.A. Bolton,[56] E.E. Boos,[37] G. Borissov,[41] T. Bose,[59] A. Brandt,[76] O. Brandt,[23] R. Brock,[62] G. Brooijmans,[68] A. Bross,[47] D. Brown,[17] J. Brown,[17] X.B. Bu,[7] D. Buchholz,[50] M. Buehler,[79] V. Buescher,[24] V. Bunichev,[37] S. Burdin[b],[41] T.H. Burnett,[80] C.P. Buszello,[42] B. Calpas,[15] E. Camacho-Pérez,[32] M.A. Carrasco-Lizarraga,[32] B.C.K. Casey,[47] H. Castilla-Valdez,[32] S. Chakrabarti,[70] D. Chakraborty,[49] K.M. Chan,[53] A. Chandra,[78] G. Chen,[55] S. Chevalier-Théry,[18] D.K. Cho,[75] S.W. Cho,[31] S. Choi,[31] B. Choudhary,[28] T. Christoudias,[42] S. Cihangir,[47] D. Claes,[64] J. Clutter,[55] M. Cooke,[47] W.E. Cooper,[47] M. Corcoran,[78] F. Couderc,[18] M.-C. Cousinou,[15] A. Croc,[18] D. Cutts,[75] M. Ćwiok,[30] A. Das,[44] G. Davies,[42] K. De,[76] S.J. de Jong,[34] E. De La Cruz-Burelo,[32] F. Déliot,[18] M. Demarteau,[47] R. Demina,[69] D. Denisov,[47] S.P. Denisov,[38] S. Desai,[47] K. DeVaughan,[64] H.T. Diehl,[47] M. Diesburg,[47] A. Dominguez,[64] T. Dorland,[80] A. Dubey,[28] L.V. Dudko,[37] D. Duggan,[65] A. Duperrin,[15] S. Dutt,[27] A. Dyshkant,[49] M. Eads,[64] D. Edmunds,[62] J. Ellison,[45] V.D. Elvira,[47] Y. Enari,[17] S. Eno,[58] H. Evans,[51] A. Evdokimov,[71] V.N. Evdokimov,[38] G. Facini,[60] T. Ferbel,[58,69] F. Fiedler,[24] F. Filthaut,[34] W. Fisher,[62] H.E. Fisk,[47] M. Fortner,[49] H. Fox,[41] S. Fuess,[47] T. Gadfort,[71] A. Garcia-Bellido,[69] V. Gavrilov,[36] P. Gay,[13] W. Geist,[19] W. Geng,[15,62] D. Gerbaudo,[66] C.E. Gerber,[48] Y. Gershtein,[65] G. Ginther,[47,69] G. Golovanov,[35] A. Goussiou,[80] P.D. Grannis,[70] S. Greder,[19] H. Greenlee,[47] Z.D. Greenwood,[57] E.M. Gregores,[4] G. Grenier,[20] Ph. Gris,[13] J.-F. Grivaz,[16] A. Grohsjean,[18] S. Grünendahl,[47] M.W. Grünewald,[30] F. Guo,[70] J. Guo,[70] G. Gutierrez,[47] P. Gutierrez,[73] A. Haas[c],[68] S. Hagopian,[46] J. Haley,[60] L. Han,[7] K. Harder,[43] A. Harel,[69] J.M. Hauptman,[54] J. Hays,[42] T. Head,[43] T. Hebbeker,[21] D. Hedin,[49] H. Hegab,[74] A.P. Heinson,[45] U. Heintz,[75] C. Hensel,[23] I. Heredia-De La Cruz,[32] K. Herner,[61] G. Hesketh,[60] M.D. Hildreth,[53] R. Hirosky,[79] T. Hoang,[46] J.D. Hobbs,[70] B. Hoeneisen,[12] M. Hohlfeld,[24] S. Hossain,[73] Z. Hubacek,[10] N. Huske,[17] V. Hynek,[10] I. Iashvili,[67] R. Illingworth,[47] A.S. Ito,[47] S. Jabeen,[75] M. Jaffré,[16] S. Jain,[67] D. Jamin,[15] R. Jesik,[42] K. Johns,[44] M. Johnson,[47] D. Johnston,[64] A. Jonckheere,[47] P. Jonsson,[42] J. Joshi,[27] A. Juste[d],[47] K. Kaadze,[56] E. Kajfasz,[15] D. Karmanov,[37] P.A. Kasper,[47] I. Katsanos,[64] R. Kehoe,[77] S. Kermiche,[15] N. Khalatyan,[47] A. Khanov,[74] A. Kharchilava,[67] Y.N. Kharzheev,[35] D. Khatidze,[75] M.H. Kirby,[50] J.M. Kohli,[27] A.V. Kozelov,[38] J. Kraus,[62] A. Kumar,[67] A. Kupco,[11] T. Kurča,[20] V.A. Kuzmin,[37] J. Kvita,[9] S. Lammers,[51] G. Landsberg,[75] P. Lebrun,[20] H.S. Lee,[31] S.W. Lee,[54] W.M. Lee,[47] J. Lellouch,[17] L. Li,[45] Q.Z. Li,[47] S.M. Lietti,[5] J.K. Lim,[31] D. Lincoln,[47] J. Linnemann,[62] V.V. Lipaev,[38] R. Lipton,[47] Y. Liu,[7] Z. Liu,[6] A. Lobodenko,[39] M. Lokajicek,[11] P. Love,[41] H.J. Lubatti,[80] R. Luna-Garcia[e],[32] A.L. Lyon,[47] A.K.A. Maciel,[2] D. Mackin,[78] R. Madar,[18] R. Magaña-Villalba,[32] S. Malik,[64] V.L. Malyshev,[35] Y. Maravin,[56] J. Martínez-Ortega,[32] R. McCarthy,[70] C.L. McGivern,[55] M.M. Meijer,[34] A. Melnitchouk,[63] D. Menezes,[49] P.G. Mercadante,[4] M. Merkin,[37] A. Meyer,[21] J. Meyer,[23] N.K. Mondal,[29] G.S. Muanza,[15] M. Mulhearn,[79] E. Nagy,[15] M. Naimuddin,[28] M. Narain,[75] R. Nayyar,[28] H.A. Neal,[61] J.P. Negret,[8] P. Neustroev,[39] S.F. Novaes,[5] T. Nunnemann,[25] G. Obrant,[39] J. Orduna,[32] N. Osman,[42] J. Osta,[53] G.J. Otero y Garzón,[1] M. Owen,[43] M. Padilla,[45] M. Pangilinan,[75] N. Parashar,[52] V. Parihar,[75] S.K. Park,[31] J. Parsons,[68] R. Partridge[c],[75] N. Parua,[51] A. Patwa,[71] B. Penning,[47] M. Perfilov,[37] K. Peters,[43] Y. Peters,[43] G. Petrillo,[69] P. Pétroff,[16] R. Piegaia,[1] J. Piper,[62] M.-A. Pleier,[71] P.L.M. Podesta-Lerma[f],[32] V.M. Podstavkov,[47] M.-E. Pol,[2] P. Polozov,[36] A.V. Popov,[38] M. Prewitt,[78] D. Price,[51] S. Protopopescu,[71] J. Qian,[61] A. Quadt,[23] B. Quinn,[63] M.S. Rangel,[2] K. Ranjan,[28] P.N. Ratoff,[41] I. Razumov,[38] P. Renkel,[77] P. Rich,[43] M. Rijssenbeek,[70] I. Ripp-Baudot,[19] F. Rizatdinova,[74] M. Rominsky,[47] C. Royon,[18] P. Rubinov,[47] R. Ruchti,[53] G. Safronov,[36] G. Sajot,[14] A. Sánchez-Hernández,[32] M.P. Sanders,[25] B. Sanghi,[47] A.S. Santos,[5] G. Savage,[47] L. Sawyer,[57] T. Scanlon,[42] R.D. Schamberger,[70] Y. Scheglov,[39] H. Schellman,[50] T. Schliephake,[26] S. Schlobohm,[80] C. Schwanenberger,[43] R. Schwienhorst,[62] J. Sekaric,[55] H. Severini,[73] E. Shabalina,[23] V. Shary,[18] A.A. Shchukin,[38] R.K. Shivpuri,[28] V. Simak,[10] V. Sirotenko,[47] P. Skubic,[73] P. Slattery,[69] D. Smirnov,[53] K.J. Smith,[67] G.R. Snow,[64] J. Snow,[72] S. Snyder,[71] S. Söldner-Rembold,[43] L. Sonnenschein,[21] A. Sopczak,[41] M. Sosebee,[76] K. Soustruznik,[9] B. Spurlock,[76] J. Stark,[14] V. Stolin,[36] D.A. Stoyanova,[38] E. Strauss,[70] M. Strauss,[73] D. Strom,[48] L. Stutte,[47] P. Svoisky,[73] M. Takahashi,[43] A. Tanasijczuk,[1] W. Taylor,[6] M. Titov,[18] V.V. Tokmenin,[35] D. Tsybychev,[70] B. Tuchming,[18] C. Tully,[66] P.M. Tuts,[68] L. Uvarov,[39] S. Uvarov,[39] S. Uzunyan,[49] R. Van Kooten,[51] W.M. van Leeuwen,[33] N. Varelas,[48] E.W. Varnes,[44] I.A. Vasilyev,[38] P. Verdier,[20] L.S. Vertogradov,[35] M. Verzocchi,[47] M. Vesterinen,[43] D. Vilanova,[18] P. Vint,[42] P. Vokac,[10] H.D. Wahl,[46] M.H.L.S. Wang,[69] J. Warchol,[53] G. Watts,[80] M. Wayne,[53] M. Weber[g],[47] L. Welty-Rieger,[50] M. Wetstein,[58] A. White,[76] D. Wicke,[24] M.R.J. Williams,[41] G.W. Wilson,[55] S.J. Wimpenny,[45] M. Wobisch,[57] D.R. Wood,[60] T.R. Wyatt,[43] Y. Xie,[47] C. Xu,[61] S. Yacoob,[50] R. Yamada,[47] W.-C. Yang,[43] T. Yasuda,[47] Y.A. Yatsunenko,[35] Z. Ye,[47] H. Yin,[7] K. Yip,[71] H.D. Yoo,[75] S.W. Youn,[47] J. Yu,[76] S. Zelitch,[79] T. Zhao,[80] B. Zhou,[61] J. Zhu,[61] M. Zielinski,[69] D. Zieminska,[51] and L. Zivkovic[68]

(The D0 Collaboration*)

[1]*Universidad de Buenos Aires, Buenos Aires, Argentina*
[2]*LAFEX, Centro Brasileiro de Pesquisas Físicas, Rio de Janeiro, Brazil*
[3]*Universidade do Estado do Rio de Janeiro, Rio de Janeiro, Brazil*
[4]*Universidade Federal do ABC, Santo André, Brazil*
[5]*Instituto de Física Teórica, Universidade Estadual Paulista, São Paulo, Brazil*
[6]*Simon Fraser University, Vancouver, British Columbia, and York University, Toronto, Ontario, Canada*
[7]*University of Science and Technology of China, Hefei, People's Republic of China*
[8]*Universidad de los Andes, Bogotá, Colombia*
[9]*Charles University, Faculty of Mathematics and Physics, Center for Particle Physics, Prague, Czech Republic*
[10]*Czech Technical University in Prague, Prague, Czech Republic*
[11]*Center for Particle Physics, Institute of Physics, Academy of Sciences of the Czech Republic, Prague, Czech Republic*
[12]*Universidad San Francisco de Quito, Quito, Ecuador*
[13]*LPC, Université Blaise Pascal, CNRS/IN2P3, Clermont, France*
[14]*LPSC, Université Joseph Fourier Grenoble 1, CNRS/IN2P3, Institut National Polytechnique de Grenoble, Grenoble, France*
[15]*CPPM, Aix-Marseille Université, CNRS/IN2P3, Marseille, France*
[16]*LAL, Université Paris-Sud, CNRS/IN2P3, Orsay, France*
[17]*LPNHE, Universités Paris VI and VII, CNRS/IN2P3, Paris, France*
[18]*CEA, Irfu, SPP, Saclay, France*
[19]*IPHC, Université de Strasbourg, CNRS/IN2P3, Strasbourg, France*
[20]*IPNL, Université Lyon 1, CNRS/IN2P3, Villeurbanne, France and Université de Lyon, Lyon, France*
[21]*III. Physikalisches Institut A, RWTH Aachen University, Aachen, Germany*
[22]*Physikalisches Institut, Universität Freiburg, Freiburg, Germany*
[23]*II. Physikalisches Institut, Georg-August-Universität Göttingen, Göttingen, Germany*
[24]*Institut für Physik, Universität Mainz, Mainz, Germany*
[25]*Ludwig-Maximilians-Universität München, München, Germany*
[26]*Fachbereich Physik, Bergische Universität Wuppertal, Wuppertal, Germany*
[27]*Panjab University, Chandigarh, India*
[28]*Delhi University, Delhi, India*
[29]*Tata Institute of Fundamental Research, Mumbai, India*
[30]*University College Dublin, Dublin, Ireland*
[31]*Korea Detector Laboratory, Korea University, Seoul, Korea*
[32]*CINVESTAV, Mexico City, Mexico*
[33]*FOM-Institute NIKHEF and University of Amsterdam/NIKHEF, Amsterdam, The Netherlands*
[34]*Radboud University Nijmegen/NIKHEF, Nijmegen, The Netherlands*
[35]*Joint Institute for Nuclear Research, Dubna, Russia*
[36]*Institute for Theoretical and Experimental Physics, Moscow, Russia*
[37]*Moscow State University, Moscow, Russia*
[38]*Institute for High Energy Physics, Protvino, Russia*
[39]*Petersburg Nuclear Physics Institute, St. Petersburg, Russia*
[40]*Stockholm University, Stockholm and Uppsala University, Uppsala, Sweden*
[41]*Lancaster University, Lancaster LA1 4YB, United Kingdom*
[42]*Imperial College London, London SW7 2AZ, United Kingdom*
[43]*The University of Manchester, Manchester M13 9PL, United Kingdom*
[44]*University of Arizona, Tucson, Arizona 85721, USA*
[45]*University of California Riverside, Riverside, California 92521, USA*

[46] Florida State University, Tallahassee, Florida 32306, USA
[47] Fermi National Accelerator Laboratory, Batavia, Illinois 60510, USA
[48] University of Illinois at Chicago, Chicago, Illinois 60607, USA
[49] Northern Illinois University, DeKalb, Illinois 60115, USA
[50] Northwestern University, Evanston, Illinois 60208, USA
[51] Indiana University, Bloomington, Indiana 47405, USA
[52] Purdue University Calumet, Hammond, Indiana 46323, USA
[53] University of Notre Dame, Notre Dame, Indiana 46556, USA
[54] Iowa State University, Ames, Iowa 50011, USA
[55] University of Kansas, Lawrence, Kansas 66045, USA
[56] Kansas State University, Manhattan, Kansas 66506, USA
[57] Louisiana Tech University, Ruston, Louisiana 71272, USA
[58] University of Maryland, College Park, Maryland 20742, USA
[59] Boston University, Boston, Massachusetts 02215, USA
[60] Northeastern University, Boston, Massachusetts 02115, USA
[61] University of Michigan, Ann Arbor, Michigan 48109, USA
[62] Michigan State University, East Lansing, Michigan 48824, USA
[63] University of Mississippi, University, Mississippi 38677, USA
[64] University of Nebraska, Lincoln, Nebraska 68588, USA
[65] Rutgers University, Piscataway, New Jersey 08855, USA
[66] Princeton University, Princeton, New Jersey 08544, USA
[67] State University of New York, Buffalo, New York 14260, USA
[68] Columbia University, New York, New York 10027, USA
[69] University of Rochester, Rochester, New York 14627, USA
[70] State University of New York, Stony Brook, New York 11794, USA
[71] Brookhaven National Laboratory, Upton, New York 11973, USA
[72] Langston University, Langston, Oklahoma 73050, USA
[73] University of Oklahoma, Norman, Oklahoma 73019, USA
[74] Oklahoma State University, Stillwater, Oklahoma 74078, USA
[75] Brown University, Providence, Rhode Island 02912, USA
[76] University of Texas, Arlington, Texas 76019, USA
[77] Southern Methodist University, Dallas, Texas 75275, USA
[78] Rice University, Houston, Texas 77005, USA
[79] University of Virginia, Charlottesville, Virginia 22901, USA
[80] University of Washington, Seattle, Washington 98195, USA

We report the result of a search for the pair production of the lightest supersymmetric partner of the top quark ($\tilde{t}_1$) in $p\bar{p}$ collisions at a center-of-mass energy of 1.96 TeV at the Fermilab Tevatron collider corresponding to an integrated luminosity of 5.4 fb^{-1}. The scalar top quarks are assumed to decay into a b quark, a charged lepton, and a scalar neutrino ($\tilde{\nu}$), and the search is performed in the electron plus muon final state. No significant excess of events above the standard model prediction is detected, and improved exclusion limits at the 95% C.L. are set in the the ($M_{\tilde{t}_1}$,$M_{\tilde{\nu}}$) mass plane.

PACS numbers: 14.80.Ly, 13.85.Rm

Supersymmetric theories [1] predict the existence of scalar partners for each of the standard model (SM) fermions. In the minimal supersymmetric standard model (MSSM) [2], the mixing between the chiral states of the scalar partners of the SM fermions is greatest for the partners of the top quark due to its large Yukawa coupling [3]. Thus, it is possible that the scalar top quark ($\tilde{t}_1$) is the lightest squark and has the largest production cross section. If R-parity [1] is conserved, then scalar top quarks would be produced by $p\bar{p}$ collisions in pairs with the dominant processes being quark-antiquark annihilation and gluon fusion [3].

In this letter we report on a search for the production of $\tilde{t}_1\bar{\tilde{t}}_1$ pairs in the $b\bar{b}e^{\pm}\mu^{\mp}\tilde{\nu}\bar{\tilde{\nu}}$ final state. We assume that the $\tilde{t}_1$ has a 100% branching fraction in this three-body decay mode with equal fraction to each lepton type, that R-parity is conserved, and that the sneutrino ($\tilde{\nu}$) is the lightest supersymmetric particle or decays invisibly into a neutrino and a neutralino ($\tilde{\chi}^0_1$). This analysis uses data corresponding to an integrated luminosity of 5.4 fb^{-1} collected using the D0 detector operating at the Fermilab Tevatron collider at $\sqrt{s} = 1.96$ TeV. The data were collected from April 2002 through June 2009. The D0 Collaboration has previously searched [4–6] for top squark

*with visitors from [a]Augustana College, Sioux Falls, SD, USA, [b]The University of Liverpool, Liverpool, UK, [c]SLAC, Menlo Park, CA, USA, [d]ICREA/IFAE, Barcelona, Spain, [e]Centro de Investigacion en Computacion - IPN, Mexico City, Mexico, [f]ECFM, Universidad Autonoma de Sinaloa, Culiacán, Mexico, and [g]Universität Bern, Bern, Switzerland.

pair production in the final states $b\bar{b}\ell^{\pm}\ell^{\mp}\tilde{\nu}\bar{\tilde{\nu}}$ where the lepton pair is ee, $\mu\mu$, or $e\mu$. Two of these earlier searches used subsets of this data set corresponding to integrated luminosities of 0.43 fb^{-1} and 1.1 fb^{-1}, while the earliest search used data from the Tevatron Run I, corresponding to an integrated luminosity of 0.11 fb^{-1}. Searches for top squark pair production in the $b\bar{b}\ell^{\pm}\ell^{\mp}\tilde{\nu}\bar{\tilde{\nu}}$ final states have also been reported by the CDF collaboration [7] and by the ALEPH, L3, and OPAL Collaborations [8].

The main components of the D0 detector [9] include a central tracking system located inside a 2 T superconducting solenoid. The inner-most tracking element is the silicon microstrip tracker (SMT), followed by a scintillating fiber tracker. These two detectors together measure the momenta of charged particles. The tracking system provides full coverage in the azimuthal (ϕ) direction for $|\eta| < 2$, where the pseudorapidity η is defined as $\eta = -\ln(\tan\theta/2)$ and θ is the polar angle with respect to the proton beam direction. Outside the solenoid is the uranium/liquid argon calorimeter which is divided into a central calorimeter and two end-cap calorimeters. Each of these three calorimeters have electromagnetic layers followed by hadronic layers. The outermost component of the detector is the muon system, which consists of proportional drift tubes and scintillator trigger counters, followed by 1.8 T iron toroids and two additional layers of drift tubes and scintillators. Events are selected for offline analysis by a three-level trigger system. All events are required to pass one of a suite of single-electron triggers or single-muon triggers using information from the tracking system, the calorimeter, and the muon system.

For each event, a primary $p\bar{p}$ interaction vertex is defined. If more than one vertex is reconstructed, the primary vertex is taken to be the vertex least consistent with originating from a soft collision. The location of the primary vertex along the beam direction is required to be within ±60 cm of the detector center.

Jets are reconstructed using the D0 Run II cone algorithm [10] with cone of radius $\mathcal{R} \equiv \sqrt{(\Delta\phi)^2 + (\Delta y)^2} < 0.5$, where y is the rapidity. Jet energies are calibrated using the standard D0 procedure [11]. A jet is retained in an event if it has transverse energy $E_T > 20$ GeV, $|\eta| < 2.5$, and if $\Delta\mathcal{R}(\text{jet,electron}) = \sqrt{(\Delta\phi)^2 + (\Delta\eta)^2} > 0.5$. No requirement on the number of jets is applied.

Electrons are required to have transverse momentum $p_T^e > 15$ GeV and $|\eta| < 1.1$. They are required to be isolated, defined as having $[E_{tot}(0.4) - E_{EM}(0.2)]/E_{EM}(0.2) < 0.15$ where $E_{tot}(0.4)$ is the total calorimeter energy in a cone of radius $\mathcal{R} = 0.4$ and $E_{EM}(0.2)$ is the electromagnetic energy in a cone of radius $\mathcal{R} = 0.2$. In addition, the shower development in the calorimeter is required to be consistent with that of an electromagnetic shower both transversely and longitudinally. An eight-variable likelihood function is constructed to further distinguish between electromagnetic and hadronic showers. The output of this function ranges from 0 to 1, and electrons are required to have a likelihood value greater than 0.85. Electromagnetic showers associated with electrons are also required to match a central track within $\Delta\eta < 0.05$ and $\Delta\phi < 0.05$ of the electromagnetic cluster.

Muons are required to have transverse momentum $p_T^{\mu} > 10$ GeV and $|\eta| < 2$. They are required to have both drift tube and scintillator hits in the muon system and to match a track in the central tracker. If the central track includes hits in the SMT, the distance of closest approach (DCA) between the muon track and the primary vertex is required to be less than 0.02 cm. If there are no SMT hits, then the DCA is required to be less than 0.2 cm. Muons are also required to satisfy isolation requirements in both the calorimeter and the central tracker. For the calorimeter isolation, the transverse energy in the cone $\mathcal{R} < 0.5$ around the muon track divided by p_T^{μ} must be less than 0.15. For the central tracker isolation, the sum of the transverse energy of the tracks in the hollow cone $0.1 < \mathcal{R} < 0.5$ divided by p_T^{μ} must be less than 0.15.

Events are required to have exactly one electron and one muon with opposite charge and to have a minimum separation between the electron and the muon $\Delta\mathcal{R}(e,\mu) > 0.5$. The missing transverse energy ($\not\!\!E_T$) is calculated from the calorimeter energy corrected for the jet and electron calibrations. It is then adjusted to account for the transverse momentum of the muon. All retained events are required to have $\not\!\!E_T > 7$ GeV. We refer to this preliminary set of selection requirements as the preselection.

Signal Monte Carlo (MC) events are generated in a 2-D grid, i.e., for $\tilde{t}_1$ masses ranging from 100 GeV to 240 GeV, and for $\tilde{\nu}$ masses ranging from 40 GeV to 140 GeV, each in 10 GeV steps. For each point, the MSSM decay parameters are calculated with SUSPECT [12] and SDECAY [13]. MADGRAPH/MADEVENT [14] is used to generate four-vectors for the signal events with PYTHIA [15] providing the showering and hadronization. The next-to-leading order (NLO) cross section for $\tilde{t}_1$ pair production is calculated by PROSPINO 2.0 [16] with the CTEQ6.1M [17] parton distribution functions (PDFs). The calculations are performed with the factorization and renormalization scales set to one, one half, and two times the $\tilde{t}_1$ mass to determine the nominal value and the negative and positive uncertainties. The scale factor uncertainties are combined quadratically with the PDF uncertainties [17, 18] to give the total theoretical uncertainties for the signal cross sections.

The dominant SM backgrounds for this decay are $Z/\gamma^* \to \tau\tau$ with $\tau \to l\nu$; diboson production including WW, WZ, and ZZ; top quark pairs; W + jets; and instrumental background coming from multijet (MJ) processes where jets are misidentified as electrons or contain muons that pass the isolation criterion and with $\not\!\!E_T$ arising from energy mismeasurement. All the background processes in this analysis except for MJ are modeled using MC simulation. Vector boson pair production is simulated with PYTHIA, while all other backgrounds are simulated at the parton level with ALPGEN [19], with PYTHIA used for hadronization and showering. In order to simulate detector noise and multiple $p\bar{p}$ interaction effects, each MC event is overlayed with a data event from randomly chosen $p\bar{p}$ crossings.

MC correction factors determined from data are applied to make distributions consistent between data and MC. These corrections include factors for the luminosity profile, beam spot position, muon and electron identification efficiencies, boson transverse momentum, and jet, electron, and muon energy resolutions.

The MJ background is estimated from a selection of data events not overlapping with the search sample and is selected by inverting the electron likelihood and muon isolation requirements. This sample is used to determine the shape of the MJ background. Because most same-sign di-lepton events come from MJ processes, we obtain the normalization factor by taking the ratio of the number of same-sign events that pass the likelihood and isolation requirements to the number of same-sign events that fail these requirements. To remove W+jet events from the MJ same-sign sample, we make the additional requirement $\not\!\!E_T < 20$ GeV, since W+jets events tend to have large $\not\!\!E_T$. We also correct this ratio for non-MJ SM processes that produce like-sign leptons, using the MC samples.

Data events are required to satisfy at least one of a suite of single-electron or single-muon triggers. The efficiency of the combination of the single-electron triggers is measured using a subset of the search sample in which at least one of the single-muon triggers fired, and vice-versa for the single muon triggers. The combination of these two efficiencies, taken to be the overall trigger efficiency, is then applied as a correction to the MC samples.

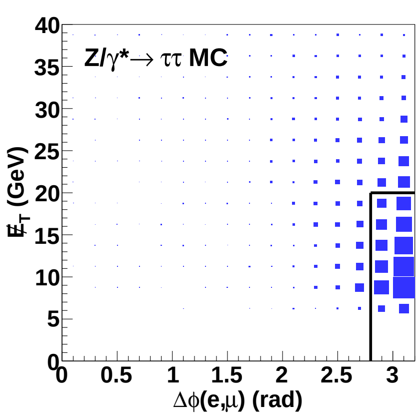

FIG. 1: (color online) $\not\!\!E_T$ versus $\Delta\phi(e,\mu)$ for $Z/\gamma^* \to \tau\tau$ MC events. Events inside the black box in the lower right corner are removed. The sizes of the boxes are proportional to the number of events in the underlying cell.

The mass difference, $\Delta M = M_{\tilde{t}_1} - M_{\tilde{\nu}}$ determines the kinematics of the final state. A larger ΔM will lead, on average, to larger $\not\!\!E_T$, larger jet energy, and higher p_T charged leptons. We divide the range of ΔM into a "large-ΔM" region ($\Delta M > 60$ GeV) and "small-ΔM" region ($\Delta M <$60 GeV). To illustrate these regions, we have chosen two benchmark points, $(M_{\tilde{t}_1}, M_{\tilde{\nu}})$ = (200 GeV, 100 GeV) and (110 GeV, 90 GeV), which will be referred to as the large-ΔM and small-ΔM benchmarks, respectively. Since there are many signal points and their characteristics differ significantly, the analysis strategy is to optimize the signal selection as a function of ΔM.

For all values of ΔM, the largest background after preselection is $Z/\gamma^* \to \tau\tau$. A two-dimensional plot of the azimuthal angle between the electron and muon, $\Delta\phi(e,\mu)$, vs. $\not\!\!E_T$ for $Z/\gamma^* \to \tau\tau$ MC events is shown in Fig. 1. The two leptons from $Z/\gamma^* \to \tau\tau$ tend to be back-to-back in ϕ, and tend to have low $\not\!\!E_T$. We therefore reject events in which $\Delta\phi(e,\mu) > 2.8$ and $\not\!\!E_T < 20$ GeV and label this as "Selection 1".

Figure 2 compares $\not\!\!E_T$, electron p_T, and muon p_T of the data and the sum of all backgrounds at this stage of the analysis. The agreement confirms our understanding of the SM backgrounds, of the trigger efficiency, and of other MC corrections. After selection 1, the three largest backgrounds are $Z/\gamma^* \to \tau\tau$, WW, and $t\bar{t}$ production. To discriminate these backgrounds from signal we create for each of them a composite discriminant variable from a linear combination of kinematic quantities. We use the R software package [20] to calculate the maximum likelihood coefficients $\vec{\beta}$ for a generalized linear model (GLM) [21] of the form

$$\delta A = \ln \frac{\mu}{1-\mu} = \beta_0 + \vec{\beta} \cdot \vec{X} \qquad (1)$$

to discriminate between signal and a specific background source A. Here, μ is the probability that an event is signal, β_0 is a constant, $\vec{\beta}$ is the vector of coefficients, and $\vec{X}$ is the vector of event kinematic variables. By construction, $\delta A = 0$ when $\mu = 0.5$, and signal-like events have positive δA. The discriminant δZ is constructed to separate signal from $Z/\gamma^* \to \tau\tau$ background, using an equal number of signal and $Z/\gamma^* \to \tau\tau$ MC events to determine the coefficients β_0 and $\vec{\beta}$. For $\vec{X}$ we use the following variables: $\ln(\not\!\!E_T)$, $\ln(p_T^\mu)$, $\ln(p_T^e)$, $\Delta\phi(e,\mu)$, $\Delta\phi(e,\not\!\!E_T)$, $\Delta\phi(\mu,\not\!\!E_T)$, and $\Delta\phi(e,\not\!\!E_T) \times \Delta\phi(\mu,\not\!\!E_T)$. For each value of ΔM, ranging from 20 to 200 GeV, we use the same variables with re-optimized coefficients. We use a similar method for creating the discriminants δWW and $\delta t\bar{t}$ to separate signal from WW and $t\bar{t}$ backgrounds. For δWW we use the variables $\ln(\not\!\!E_T)$, $\ln(p_T^\mu)$, $\ln(p_T^e)$, number of jets, $\Delta\phi(e,\mu)$, and $\ln(WW_{\rm tag})$. Here $WW_{\rm tag}$ is the magnitude of the vector sum of p_T^e, p_T^μ, and $\not\!\!E_T$, which should be close to zero for WW events. For $\delta t\bar{t}$, we use the variables $\ln(\not\!\!E_T)$, $\ln(p_T^\mu)$, $\ln(p_T^e)$, $\ln(1+H_T)$, the

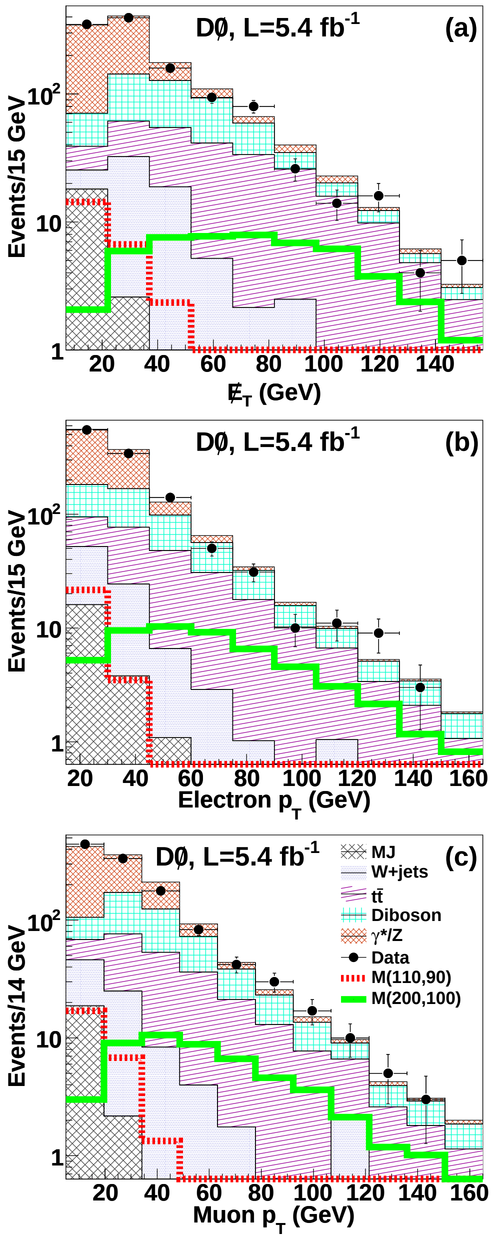

FIG. 2: (color online) Distribution of (a) $\not\!\!E_T$, (b) electron p_T, and (c) muon p_T comparing data and all background processes after Selection 1. The thick dashed and thick solid lines represent the small-ΔM and large-ΔM signal benchmarks, respectively.

energy of the second most energetic jet, and $WW_{\rm tag}$. The variable H_T is the scalar sum of the transverse energies of all jets in an event.

We first apply a requirement using the most effective discriminator of the three. For $\Delta M < 60$ GeV, we require $\delta t\bar{t} > 0$. The efficiency of this requirement is 0.95 for the small-ΔM signal benchmark and 0.03 for $t\bar{t}$. For $\Delta M \geq 60$ GeV, we require $\delta Z > 0$. The efficiency of this requirement is 0.96 for the large-ΔM signal benchmark and 0.01 for $Z/\gamma^* \to \tau\tau$. After making these requirements on one variable, we build 2-D distributions of the two remaining discriminants. Figure 3 shows these distributions for the small-ΔM benchmark signal and the two most significant remaining backgrounds. In calculating the signal exclusion confidence limits, we use only the bins in the upper right quadrant where the signal is concentrated.

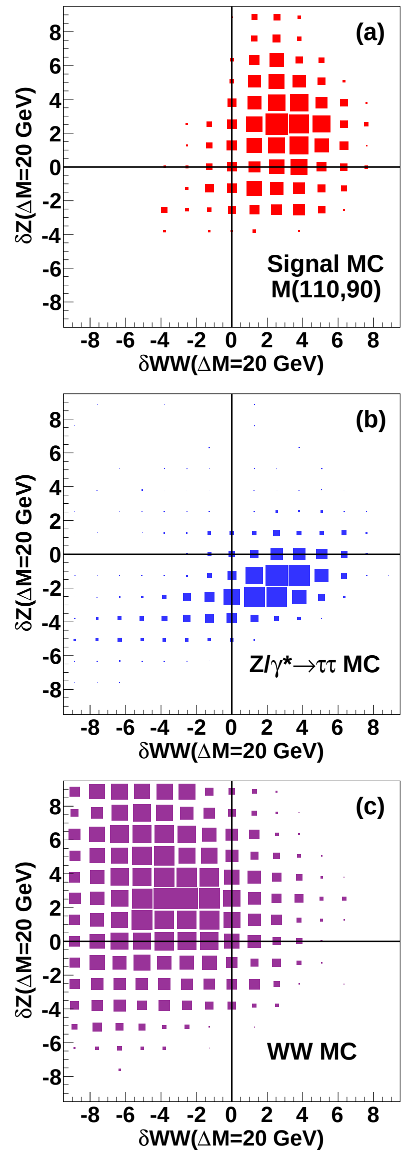

FIG. 3: (color online) Distribution of δZ versus δWW for (a) the small-ΔM signal benchmark, $(M_{\tilde{t}_1}, M_{\tilde{\nu}})$ = (110 GeV, 90 GeV), MC events, (b) $Z/\gamma^* \to \tau\tau$ MC events, and (c) WW MC events. The top right quadrant is used in the limit-setting procedure.

Table I summarizes the expected backgrounds, the expected signal, the observed data events, and the selection efficiencies.

The theoretical uncertainties on the signal cross section are approximately 20% as discussed above and are the

Sample	Preselection Events	Selection 1 Events	Selection 2 $\delta t\bar{t} > 0$ Events	Selection 2 $\delta Z > 0$ Events
$Z \to \tau\tau$	1516 ± 150	582 ± 61	515 ± 54	17.3 ± 2.0
$Z \to \mu\mu$	33.1 ± 4.7	22.9 ± 3.7	16.3 ± 2.9	5.5 ± 1.2
$Z \to ee$	23.2 ± 3.9	16.6 ± 3.0	10.2 ± 2.2	0.1 ± 2.3
WZ	12.7 ± 1.6	12.0 ± 1.5	6.3 ± 0.8	9.3 ± 1.2
WW	295 ± 32	268 ± 30	157 ± 18	237 ± 26
ZZ	2.2 ± 0.3	2.0 ± 0.3	1.0 ± 0.15	1.1 ± 0.16
$t\bar{t}$	206 ± 28	204 ± 28	6.6 ± 0.9	179 ± 24
W	70 ± 9.2	67.5 ± 9.0	55 ± 7.7	53 ± 7.4
MJ	33 ± 9.2	19.7 ± 5.5	18.4 ± 5.1	1.3 ± 0.35
Background total	2191 ± 160	1195 ± 73	785 ± 57	513 ± 37
Data	2168	1147	776	472
Small-ΔM Benchmark (110 GeV,90 GeV)	35 ± 5.6	25.5 ± 4.2	23.8 ± 3.9	-
Large-ΔM Benchmark (200 GeV,100 GeV)	55 ± 9.3	53.4 ± 9.0	-	51.8 ± 8.7

TABLE I: Expected numbers of background and signal events, and the number of events observed in the data at each stage of the analysis. The errors include statistical and systematic uncertainties. For $\Delta M < 60$ GeV, Selection 2 is $\delta t\bar{t}(\Delta M = 20$ GeV$) > 0$, and for $\Delta M \geq 60$ GeV, Selection 2 is $\delta Z(\Delta M = 100$ GeV$) > 0$.

dominant uncertainties in this analysis. The uncertainty on the integrated luminosity is 6.1%. Other systematic uncertainties included in the limit setting calculations are the lepton identification and track matching efficiencies (5%), the MJ background (27%) scale factor, the jet energy calibration (1–2)%, and the production cross section uncertainties on all the SM background processes (3–10)%. All uncertainties except for those on the MJ background and the SM production cross sections are treated as fully correlated. All systematic uncertainties are included in the limit calculations with Gaussian distributions [22].

For $\Delta M < 60$ GeV, we use the two dimensional histograms of the positive values of δZ and δWW in the limit setting procedure. For $\Delta M \geq 60$ GeV, we use the positive values of $\delta t\bar{t}$ and δWW. A modified frequentist approach [23] is used to determine the 95% C.L. exclusion limits on scalar top quark production as a function of the $\tilde{\nu}$ and $\tilde{t_1}$ masses, as shown in Fig. 4. Also shown are the exclusion regions from the CERN LEP experiments [8], previous D0 searches [5, 6], and a CDF search [7].

In conclusion, we set 95% C.L. exclusion limits on the cross section for scalar top quark pair production assuming a 100% branching fraction to $b\bar{b}l^{\pm}l^{\mp}\tilde{\nu}\bar{\tilde{\nu}}$ using 5.4 fb^{-1} of integrated luminosity from the D0 experiment at the Fermilab Tevatron collider. We have excluded stop pair production for $M_{\tilde{t}_1} < 210$ GeV when $M_{\tilde{\nu}} < 110$ GeV and the difference $M_{\tilde{t}_1} - M_{\tilde{\nu}} > 30$ GeV. This extends the previous limits on the top squark mass by more than 40 GeV for sneutrino masses less than 90 GeV and the limits on the sneutrino mass by more than 30 GeV for top squark mass equal to 150 GeV.

We thank the staffs at Fermilab and collaborating institutions, and acknowledge support from the DOE and NSF (USA); CEA and CNRS/IN2P3 (France); FASI, Rosatom and RFBR (Russia); CNPq, FAPERJ, FAPESP and FUNDUNESP (Brazil); DAE and DST (India); Colciencias (Colombia); CONACyT (Mexico); KRF and KOSEF (Korea); CONICET and UBACyT (Argentina); FOM (The Netherlands); STFC and the Royal Society (United Kingdom); MSMT and GACR (Czech Republic); CRC Program and NSERC (Canada); BMBF and DFG (Germany); SFI (Ireland); The Swedish Research Council (Sweden); and CAS and CNSF (China).

[1] P. Fayet and S. Ferrara, Phys. Rep. **32**, 249 (1977).
[2] S. Dimopoulos and H. Georgi, Nucl. Phys. **B193**, 150 (1981).
[3] W. Beenakker *et al.*, Nucl. Phys. **B515**, 3 (1998).
[4] V.M. Abazov *et al.* (D0 Collaboration), Phys. Lett. B **659**, 500 (2008).
[5] V.M. Abazov *et al.* (D0 Collaboration), Phys. Lett. B **675**, 289 (2009).
[6] W. M. Abazov *et al.* (D0 Collaboration), Phys. Lett. B **581**, 147 (2004).
[7] CDF Collaboration, arXiv:1009.0266 (2010), submitted to Phys. Rev. D.
[8] LEP SUSY Working Group (ALEPH, DELPHI, L3, and

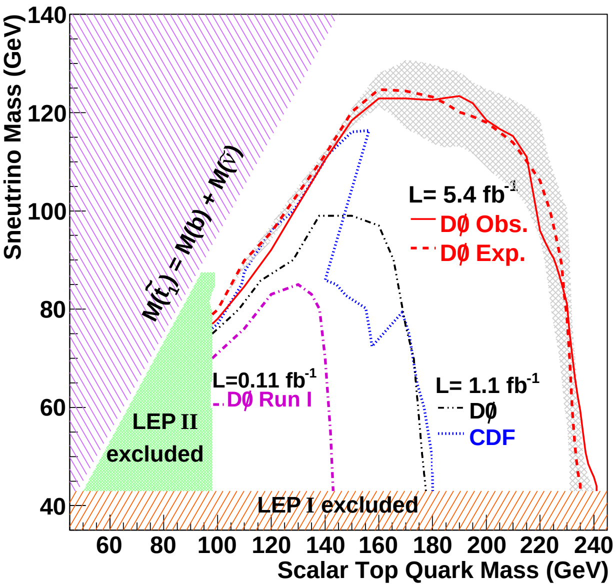

FIG. 4: (color online) The observed (expected) 95% C.L. exclusion region includes all mass points below the solid (dashed) line. The shaded band around the expected limit shows the effects of the scalar top quark pair production cross section uncertainty. The kinematically forbidden region is represented in the upper left, and the regions excluded by LEP I and LEP II [8], by previous D0 searches [5, 6], and by a previous CDF search [7] are also shown.

OPAL Collaborations), LEPSUSYWG/01-02.1 (2001), URL `http://lepsusy.web.cern.ch/lepsusy/`.

[9] W. M. Abazov *et al.* (D0 Collaboration), Nuc. Instr. Meth. Phys. Res. A **565**, 463 (2006).

[10] G. Blazey *et al.* (2000), hep-ex/0005012.

[11] J. Hegeman, J. Phys. Conf. Ser. **160**, 012024 (2009).

[12] A. Djouadi, J.-L. Kneur, and G. Moultaka, Comput. Phys. Commun. **176**, 426 (2007).

[13] M. Mühlleitner, Acta Phys. Polon. B **35**, 2753 (2004), we use version 1.1a.

[14] J. Alwall *et al.*, J. High Energy Phys. **09**, 028 (2007), we use version 4.4.13.

[15] T. Sjöstrand *et al.*, Comput. Phys. Commun. **135** (2001), we use version 6.409.

[16] W. Beenakker, R. Höpker, and M. Spira, hep-ph/9611232 (1996), we use version 2.0.

[17] J. Pumplin *et al.*, J. High Energy Phys. **07**, 012 (2002).

[18] D. Stump *et al.*, J. High Energy Phys. **10**, 046 (2003).

[19] M. Mangano *et al.*, J. High Energy Phys. **07**, 001 (2003), we use version 2.11.

[20] R Development Core Team, *R: A Language and Environment for Statistical Computing*, R Foundation for Statistical Computing, Vienna, Austria (2009), we use version 2.9.2, URL `http://www.R-project.org`.

[21] J. A. Nelder and R. W. M. Wedderburn, J. R. Statist. Soc. A **135**, 370 (1972).

[22] W. Fisher, Fermilab-TM-2386-E (2007).

[23] T. Junk, Nucl. Instr. Meth. Phys. Res. A **434**, 435 (1999).